Journal of Hydroscience and Hydraulic Engineering
Vol. 28, No.2 November, 2010, 23-35

APPLICATION OF TWO-STREAM MODEL TO ESTIMATE LEAF AREA INDEX IN THE FOREST AREA USING TERRA/ASTER DATA IN SUMMER AND WINTER

By

Yonghee Shin

The United Graduate School of Agricultural Science, Kagoshima University, Korimoto, Kagoshima, Japan

Masahiro Seguchi

Faculty of Agriculture, Saga University, Honjo-machi, Saga, Japan

and

Masumi Koriyama

Faculty of Agriculture, Saga University, Honjo-machi, Saga, Japan

SYNOPSIS

Leaf area index (LAI) is an important factor in identifying the water balance in mountainous watershed as a biological factor influencing directly on the evapotranspiration occurs in the forest area. The purpose of this study is to establish a method for LAI estimation based on the absorption and scattering process of the vertical element of electromagnetic waves and the characteristics of reflection spectrum of soil-vegetation. Firstly, we estimated the LAI in the forest area in summer and winter by applying the Terra-Advanced Spaceborne Thermal Emission and Reflection Radiometer (ASTER) data on the forested area to the LAI estimation method. Secondly, to validate the results of LAI estimation we compared them to the measured LAI obtained directly by a plant canopy analyzer at the observation points inside the target region. This study demonstrated that the LAI estimation method was a feasible and accurate method as indicated by the high relationship (r=0.97) between LAI derived from ASTER data and LAI measured directly.

INTRODUCTION

The LAI which indicates the leaf density of vegetation is defined as the total area of the all leaves (one side only) per unit horizontal ground surface area (1). LAI is an important parameter to identify the water balance and thermal environment in a forest area, because it is also a biological factor influencing on the evapotranspiration, especially, the transpiration occurs through the open stomata in leaves. The establishment of an exact estimation method of LAI is definitely necessary for the solution of environmental problems in the forest area such as desertification, deforestation, global warming etc. especially recently.

There are direct and indirect methods to determine the LAI. The direct methods are the clip method (2) by

measuring the area of leaves collected from the inside of the vegetation canopy, and the litter trap method (3) by measuring the fallen leaves into the litter trap installed on the forest floor. LAI can also be measured indirectly by using photographs taken upwards with a fish-eye lens (4) and a plant canopy analyzer (5) based on the transmission of light from the inside of the vegetation canopy. The pre-described measuring methods are on the premise of measuring the group of small area or the canopy of individual tree. However, the LAI measurement in the large area has been necessary and the development of method for estimating spatial distribution of LAI has been studied by means of satellite remote sensing technology (6, 7, 8).

Price (9) estimated the LAI of north-eastern part of Arkansas using Landsat TM bands 3 and 4 based on the two-stream approximation analysis of electromagnetic waves inside the vegetation canopy. Fassnacht et al. (10) formulated the relation between the various vegetative indexs (VI) calculated from each band of Landsat TM data and observed data of LAI to estimate the LAI at Wisconsin. Quan et al. (11) also estimated LAI using the normalized difference vegetative index (NDVI) obtained from NOAA Advanced Very High Resolution Radiometer (AVHRR), SPOT VEGETATION, and Terra Moderate Resolution Imaging Spectroradiometer (MODIS) data. The MODIS science team in the Earth Observing Program (EOS) has been produced LAI products globally and they have been updated every 8 days. The Price's method, which is based on the physical process of the electromagnetic wave inside the vegetative canopy, is excellent in its reasonability of the calculation results. However, the sufficient accuracy was not performed in the area which was examined. The above described LAI estimation methods except Price's method, were based on the relevant formulae of VI and LAI derived from the satellite data. Although the empirical vegetation index that is simple and easy, it is necessary to set many relational formulas under this condition because the relevant formulae of VI and LAI are influenced by different kinds of vegetation, season, ground surface coverage, and various of soil which make up the background. In the case of NDVI, it increases towards a certain value as LAI increases and its increase rate is high when LAI is low, but its increase rate is low in the range of high LAI value. Namely, the preciseness on the estimated value of LAI by NDVI becomes very low when LAI is higher than roughly 3 (12, 13). The problems of the pre-described methods have to be solved in order to acquire the estimation method of LAI using the satellite data which has such properties as periodicity, broadness and simultaneity. Furthermore the use of the satellite sensor data is required to replace the Landsat-5 TM sensor which creates problems caused by the aging.

The aim of this study was to establish a method for LAI estimation on the region of forest in summer and winter. First of all, the two-stream approximation model, namely, the LAI estimation method which is based on the absorption and scattering process of the vertical element of electromagnetic waves was applied. Furthermore, the characteristics of reflection spectrum of soil-vegetation system and ASTER data were examined. Next, the preciseness of the estimation method was verified by comparing the estimated result of LAI calculated by the proposed estimation method and measured result by a plant canopy analyzer (LAI-2000, Li-Cor, Nebraska, USA) in the surveyed area. Finally, the LAI estimations on the target region in summer and winter were carried out using the present method from ASTER data.

FIELD OBSERVATION AND SATELLITE DATA

Observation Areas and Methods

The observation areas of A, B, C, D were arranged as shown in Fig. 1 to measure the spectral reflectance and LAI on the soil and vegetation canopy of target region. The observation area A is the planted forest area on the foot of the mountain of Tenzan (1,046 m above sea level), where 64% of this area is covered by needle leaf trees of Japanese cedar and cypress. The observation area B and C are covered with the natural forest nearby the Nagasaki

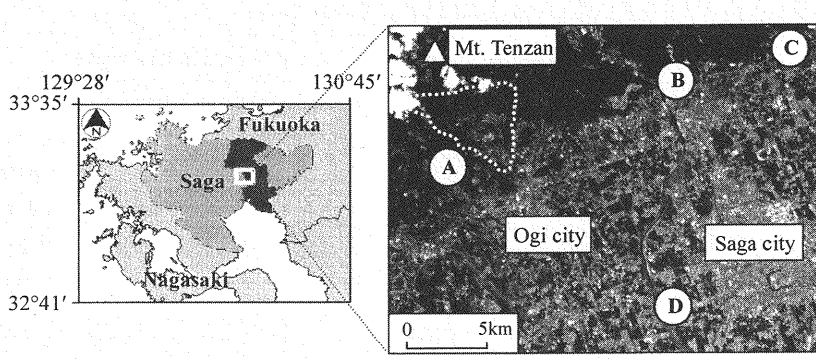

Fig. 1 Location of observation areas and study area (dotted line)

highway which mostly consist of broadleaf trees such as camphor tree and oak and the needle leaf trees such as Japanese cedar which are spread to the north of highway. On the other hand, the D observation area is the small lawn area inside the Shinrin park. Data for the LAI estimation were obtained in the upper stream area of Gion river (inside the dotted line in Fig. 1) located at the southern side of Tenzan mountain with an area approximately 12km^2 comprised of 80% and 20% forest, and agricultural and house land, respectively.

Observation of the spectral reflectance of soil and vegetation canopy was performed on the forest of broadleaf trees in the observation area B which has the highest leaf density among the observed areas. The spectral reflectance was measured by a spectrometer (LI-1800, Li-Cor, Nebraska, USA) at 11 AM ~ 2 PM on August 15, 2007 and January 6, 2008 and calculated as the ratio of spectral reflection energy from the object to that from the standard white plate. Specifically, the observation of spectral reflection energy on the vegetation canopy in the forest was performed with LI-1800 at the overlooking location to the vegetation canopy from the upper direction of mountain slope area. It was performed under the condition of front scattering on the principal horizontal plane to minimize the influence of Bidirectional Reflectance Distribution Function (BRDF) which was caused by the observing angles of the spectrometer.

On the other hand, the LAI was measured directly by LAI-2000 on the observation points inside the target area to verify the feasibility of LAI estimation result obtained from satellite data. This measurement was conducted for two weeks before and after the collecting date (August 18, 2007 and January 9, 2008) of ASTER data. The area of uniform tree species with an acreage of more than 50m×50m was selected as much as possible which correspond to the 15m×15m of spatial resolution of ASTER data. The measurement was performed in the evening or days uniformly covered with shallow clouds, because the direct solar radiation causes underestimation of the measured value of LAI (14).

Satellite Data

Advanced Spaceborne Thermal Emission and Reflection Radiometer (ASTER) sensor onboard the NASA Terra satellite provides imagery which covers a wide spectral region of the electromagnetic spectrum from visible to thermal infrared with 14 multi-spectral bands (15). The ASTER instrument consists of three separate subsystems. The visible and near-infrared (VNIR) subsystem operates in three bands (0.52 to 0.86 μm) with a spatial resolution of 15 m. Stereoscopic capability in the track path is also implemented by the 3B band in VNIR. The shortwave infrared (SWIR) subsystem operates in six bands (1.6 to 2.43 μm) with a spatial resolution of 30 m. The thermal infrared (TIR) subsystem operates in five bands (8.125 to 11.65 μm) with a spatial resolution of 90 m. The basic

Table 1. Properties of the ASTER sensor

ASTER (Advanced Spaceborne Thermal Emission and Reflection Radiometer)					
Band	VNIR (μm)	Band	SWIR (μm)	Band	TIR (μm)
1	0.52 - 0.60	4	1.600 - 1.700	10	8.125 - 8.475
2	0.63 - 0.69	5	2.145 - 2.185	11	8.475 - 8.825
3 (N)	0.76 - 0.86	6	2.185 - 2.225	12	8.925 - 9.275
3 (B)	0.76 - 0.86	7	2.235 - 2.285	13	10.25 - 10.95
		8	2.295 - 2.365	14	10.95 - 11.65
		9	2.360 - 2.430		
Spatial resolution (m)	15	30		90	
Swath width (km)	60				

characteristics of these subsystems are shown in Table 1. In this study, the satellite data were adopted from Path:113, Row:106, center: 33.11 N, 129.94 E, inclusive the part of Saga and Nagasaki which is the ASTER L1B Product. The L1B data are generated by applying these coefficients for radiometric calibrations and geometric re-sampling (16). Here, the ASTER stereo images taken during the summer (August 18, 2007) and winter (January 9, 2008) which cover the area of study were acquired. The data sets were available from the Earth Remote Sensing Data Analysis Center (ERSDAC), Japan (http://www.ersdac.or.jp/).

ESTIMATION OF LEAF AREA INDEX

Two-stream approximation model

As the processes of absorption and scattering inside the plant canopy are complicated, we used the two-stream approximation model to represent these processes (17, 18, 19) as presented in Fig.2. This model expresses the transmitting process of electromagnetic waves inside the plant canopy, covering the soil of reflectance $R_s(\lambda)$, where λ is the wavelength. The relation between the vertically downward radiation I and vertically upward radiation J at wavelength λ are expressed by Eq. 1.

$$\frac{dI}{dl} = -\alpha I + \beta J; \qquad \frac{dJ}{dl} = \alpha J - \beta I \tag{1}$$

where, α = absorption coefficient; β = scattering (reflection) coefficient; and dl = increment in leaf area index, with l measured downward from the top of the vegetation canopy which becomes l=LAI at the down most. As we define $\beta^2-\alpha^2=c^2$, the general solutions of Eq. 1 are expressed as follows:

$$I = a_1 e^{-cl} + a_2 e^{cl}; \qquad J = a_3 e^{-cl} + a_4 e^{cl} \tag{2}$$

where, c = attenuation coefficient; and a_1~a_4 = arbitrary constants. c can be obtained from measurements of the attenuation of radiation within a canopy. The following equations will be set from the boundary conditions. At the top of the vegetation canopy, we set the incident radiation to 1, namely $a_1+a_2=1$.

$$l = 0; \qquad I(0) = 1 \tag{3}$$

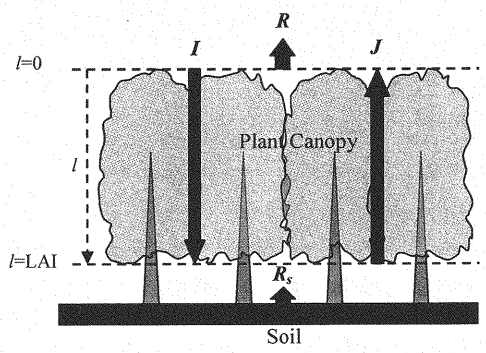

Fig. 2 A radiant energy transmission process in the canopy

At the bottom of the vegetation canopy, we consider the relation between the downward radiation and the upward radiation which is reflected from the underlying soil with reflectance $R_s(\lambda)$.

$$l = LAI \; ; \quad J(LAI) = R_s I(LAI) \tag{4}$$

where R_s = reflectance from the soils on the ground surface. The upward radiation of unit incident radiation, R is expressed as follows according to the Eq. 2, 3 and 4 when LAI=∞, namely, $R=R_\infty$ when LAI is sufficiently high (17). In addition, $R=J(0)$ as $I(0)=1$. The relation between R and LAI is given by

$$R = (R_\infty + \frac{D}{R_\infty})\frac{1}{D+1} \; ; \quad D = \frac{R_s - R_\infty}{(1/R_\infty) - R_s} e^{-2cLAI} \tag{5}$$

Application of two-stream model for LAI estimation based on ASTER data

The following formula is established between the reflectance S_i of i band observed with satellite sensor and the ground reflectance, R_i.

$$S_i = \tau_i R_i + \sigma_i \tag{6}$$

where, τ = absorption rate; and σ = reflectance of atmosphere. The following formula is devised between the S_i and the digital number of satellite data, BN_i.

$$S_i = \gamma_i BN_i + \delta_i \tag{7}$$

where, γ , δ = calibration parameters determined by ASTER i band. The Eq. 5 shall be represented in the formula of i band as follows:

$$R_{si} = \frac{\{(R_{\infty i} - R_i)/R_{\infty i} \cdot e^{2c_i LAI} + (R_i R_{\infty i} - 1)\} \cdot R_{\infty i}/(R_i R_{\infty i} - 1)}{(R_{\infty i} - R_i)/(R_i - 1/R_{\infty i}) \cdot e^{2c_i LAI} + 1} \tag{8}$$

From the Eqs. 6, 7 and 8

$$BN_{si} = \frac{BN_{\infty i} + \dfrac{(1/R_{\infty i} - q_i)(BN_i - BN_{\infty i})e^{2c_i LAI}}{1/R_{\infty i} - (p_i BN_i + q_i)}}{1 + \dfrac{p_i (BN_i - BN_{\infty i})e^{2c_i LAI}}{1/R_{\infty i} - (p_i BN_i + q_i)}} \tag{9}$$

where, $p_i = \gamma_i/\tau_i$; $q_i = (\delta_i - \sigma_i)/\tau_i$. The following formula is established between the LAI and BN_{si} because $1/R_{\infty i} >> q_i$, $p_i BN_i >> q_i$, namely, $R_{\infty i} \approx p_i BN_{\infty i}$ in the visible and near infrared wavelengths (9).

$$BN_{si} = \frac{BN_i(e^{2c_i LAI} - R_{\infty i}^2) + BN_{\infty i}(1 - e^{2c_i LAI})}{1 - R_{\infty i}^2 e^{2c_i LAI} - BN_i R_{\infty i}^2 (1 - e^{2c_i LAI})/BN_{\infty i}} \tag{10}$$

where, BN_{si} and $BN_{\infty i}$ are the ASTER data corresponding to R_s, R_∞ of i band.

Generally the reflectance of the soil on the ground surface depend largely on the types and moisture content of soils (20). Fig. 3 illustrates the changes of spectral reflectance curves according to the moisture content of Masa soil which is widely distributed in the target regions. The spectral reflectance decreased as the moisture content increased as shown in the figure. However, the relationship between R_{650} of spectral reflectance with 650 nm of visible wavelength and IR_{850} of spectral reflectance with 850 nm of near infrared wavelength is represented by a linear line called soil-line, regardless of the types and moisture contents ratio as shown in Fig. 4 (21). The soil-line is a widely researched linear relationship between the reflectance or intensity in the red and near infrared wavelengths (22, 23).

When all the soil pixels of the satellite images are placed in the red and the near infrared spectrum space, they are also distributed along a straight line. Fig. 5 illustrates the relationship between the ASTER band 2 (BN_{s2}) and band 3 (BN_{s3}) of the bare soil which can be expressed as follows:

$$BN_{s3} = a' BN_{s2} + b' \tag{11}$$

where, a'= slope; b'= intercept of this soil line. In Fig. 5, we have a'=0.82 and b'=2.0. The following formulas are established between BN_{s2} and BN_{s3} according to Eqs. 10 and 11 in case of ASTER data used in this study.

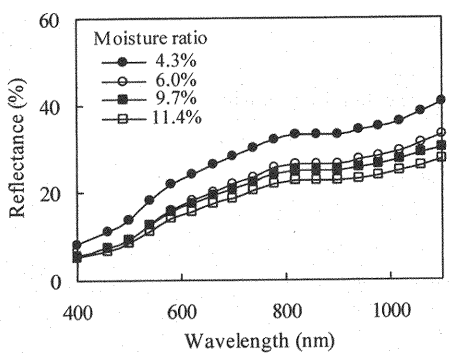

Fig. 3 Spectral reflectance curves for different water content of the Masa soil

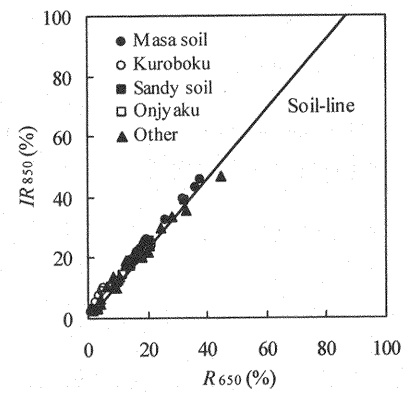

Fig. 4 Relationship between R_{650} and IR_{850}, and a Soil-line for various soils in Kyushu

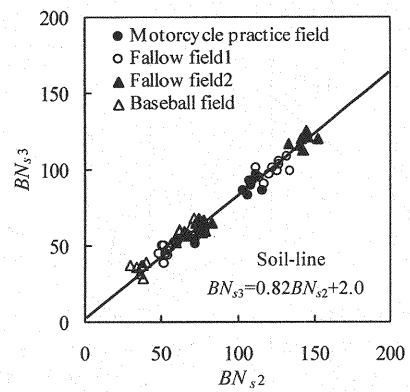

Fig. 5 Relationship between BN_{s2} and BN_{s3} of ASTER image on bare area

$$\frac{BN_3(e^{2c_3LAI}-R_{\infty 3}^2)+BN_{\infty 3}(1-e^{2c_3LAI})}{1-R_{\infty 3}^2e^{2c_3LAI}-BN_3R_{\infty 3}^2(1-e^{2c_3LAI})/BN_{\infty 3}}=a'\cdot\frac{BN_2(e^{2c_2LAI}-R_{\infty 2}^2)+BN_{\infty 2}(1-e^{2c_2LAI})}{1-R_{\infty 2}^2e^{2c_2LAI}-BN_2R_{\infty 2}^2(1-e^{2c_2LAI})/BN_{\infty 2}}+b' \quad (12)$$

$$(A_3C_2-a'A_2C_3-b'C_3C_2)(b_3b_2)^{LAI}+(B_3C_2-a'A_2D_3-b'C_2D_3)b_2^{\ LAI}$$
$$+(A_3D_2-a'B_2C_3-b'C_3D_2)b_3^{\ LAI}+(B_3D_2-a'B_2D_3-b'D_3D_2)=0 \quad (13)$$

where, $A_i=(a_i-d_i)d_i$; $B_i=(d_i-a_ie_i)d_i$; $C_i=(a_i-d_i)e_i$; $D_i=d_i-a_ie_i$; $a_i=BN_i$; $b_i=e^{2c_i}$; $d_i=BN_{\infty i}$; $e_i=R^2_{\infty i}$; $i=2$, 3. Accordingly, the LAI are derived by solving the equation with the unknown variable of LAI by substituting the parameters into Eq. 13. In addition, the parameter of the LAI estimation formula was estimated from ASTER data or obtained from *in situ* measurements and experiments in the forest areas.

Validation of the mensuration

By plotting BN_2 and BN_3 of ASTER data, the highest estimated P of scatterdiagrams shown in Fig. 6 was obtained with $BN_{\infty 2}$=44 and $BN_{\infty 3}$=180 in summer, and $BN_{\infty 2}$=25, $BN_{\infty 3}$=82 in winter which were obtained in the highest leaf density area on the study target region (see Fig. 6). The $R_{\infty 2}$=0.03, $R_{\infty 3}$=0.48 in summer and $R_{\infty 2}$=0.07,

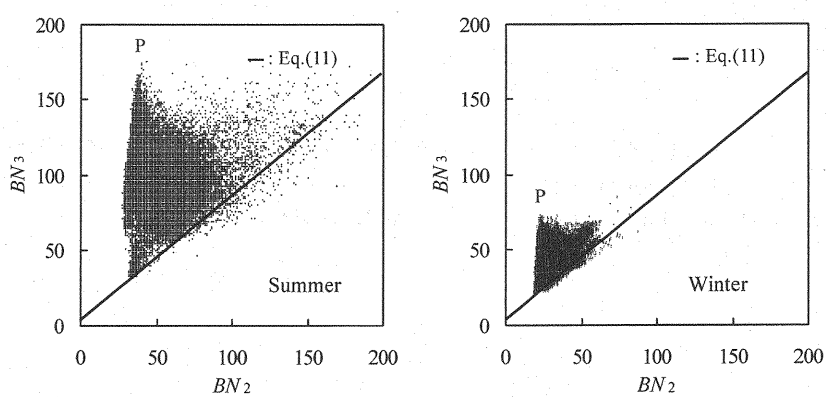

Fig. 6 Scatter diagram of ASTER image BN_2 and BN_3 within the study area

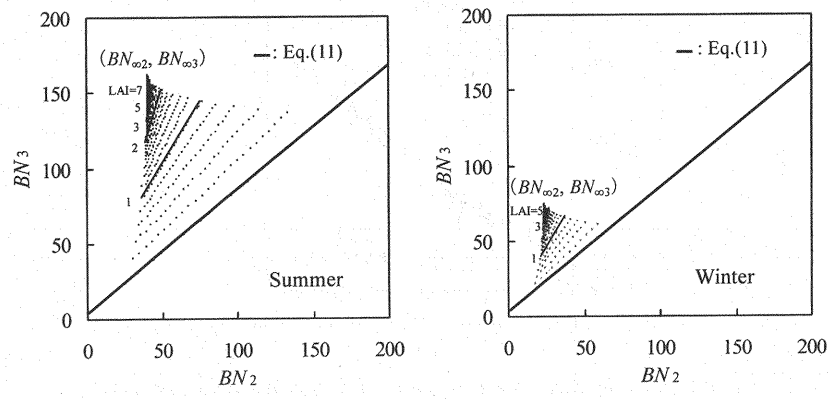

Fig. 7 Scatter diagram of BN_2 and BN_3 which calculated for each LAI

$R_{\infty 3}$=0.42 in winter were obtained by measuring the reflectance on the broadleaf forest area of B observation area which has the highest leaf density among other observation areas in this study (see Fig. 1). Furthermore, the attenuation coefficient c was obtained from the experiment which indicated the attenuation degree of absorption and scattering by the group of leaves for the radiation energy passing inside the vegetation canopy. The c_2=0.6, c_3=0.2 in summer and c_2=0.3, c_3=0.1 in winter were applied in this study.

The distribution characteristics of the relationship between BN_2 and BN_3 for each LAI values were showed in Fig. 7. The distribution was obtained by plotting the BN_2 and BN_3 calculated for the arbitrary values of LAI and BN_{si} in the Eq. 10. The distribution characteristics are mostly coincident as depicted in Fig. 6 and Fig. 7. However, the scattered diagram in Fig. 7 distributes wider than that of Fig. 6, when the LAI is less than 1. The reason for this is that the premise of the two-stream approximation model, e.g. the condition that the vegetation canopy covers the soil totally was not satisfied as the LAI gets lower. Consequently, it is thought that Eq. 10 is appropriate to estimate LAI values more than 2.

To verify the estimation method, the spectral reflection energy $L_k(\lambda)$ of an oak on various LAI was measured by LI-1800 in the experiment field of Department of Agriculture, Saga University on August 9, 2007. Fig. 8 shows the spectral reflection energy $L'_k(\lambda)$ after calibrating the differences of spectral reflection energy according to the elapse of measuring time using the Eq. 14.

$$L'_k(\lambda) = L_k(\lambda)\frac{W_0(\lambda)}{W(\lambda)} \tag{14}$$

where, $W_0(\lambda)$ = spectral reflection energy of standard reflection plate at culmination; $W(\lambda)$ = spectral reflection energy of standard reflection plate at the measurement of $L_k(\lambda)$. $L'_k(\lambda)$, which has the following relation to BN_i of ASTER data in i band (24), tends to be diminished at the range of visible wavelength as LAI increases.

$$BN_i = (\overline{L'_{ki}} - e_0)/e_1 \tag{15}$$

$$\overline{L'_{k2}} = \frac{1}{60}\int_{630}^{690} L'_k(\lambda)d\lambda \tag{16}$$

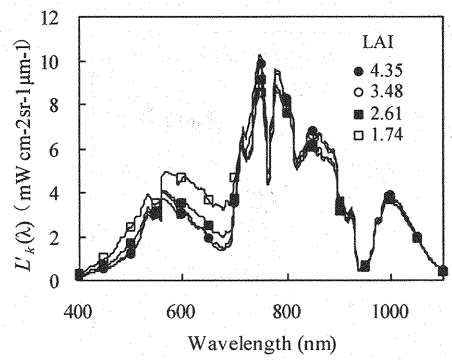

Fig. 8 Spectral reflection energy curves at various LAIs of oak

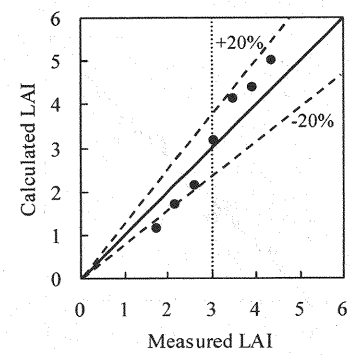

Fig. 9 Comparison of measured LAI and calculated one based on the spectral reflection energy of oak

$$\overline{L'_{k3}} = \frac{1}{100}\int_{760}^{860} L'_k(\lambda)d\lambda \qquad (17)$$

where, e_0 and e_1 are the coefficients on the offset and gain of ASTER sensor, e_0=-0.1; e_1=0.0708 for BN_2, e_0=-0.1; e_1=0.0862 for BN_3. The unit of $L'_k(\lambda)$ is [mW cm^{-2} sr^{-1} μm^{-1}]. The calculated LAI was derived from the application of the LAI estimation method using the spectral reflection energy, reflectance and other parameters obtained from the experiment. Fig. 9 shows a comparison between calculated LAI and measured LAI by clip method. As shown in Fig. 9, the calculated LAI is higher than measured one in case of LAI>3, inversely, the calculated LAI is lower than measured one in case of LAI<3. However, the difference between the calculated and measured LAI is comparatively low within ±20% usually. It is thought that the difference between the measured and calculated LAI occurs by setting the attenuation coefficient, c in constant value (LAI=3 and the slope of leave is horizontal) which depends on the variations of three dimensional array of the group of leaves.

RESULTS AND DISCUSSION

In this study, a method for LAI estimation in the wide range of forest area from ASTER data of Terra satellite was examined based on the electromagnetic wave absorption and scattering process inside the vegetation canopy. The scattered diagrams of (BN_2, BN_3) obtained from Eq. 10 were mostly coincident with the scattered diagrams obtained from ASTER data, indicating the validity of the estimation. To verify the preciseness of the estimation method, we compared calculated LAI from the ASTER data with the measured LAI at specific observation points in the forest area. Fig. 10 illustrates the comparison between the calculated LAI using the false position method by applying the BN_2, BN_3 of ASTER data in winter and summer to the LAI estimation method, and the measured LAI using a plant canopy analyzer (LAI-2000) on 16 observation points in the same seasons. As shown in Fig. 10, the calculated LAI and measured LAI have a high correlation coefficient (r=0.97) and almost agree. The root mean square error (RMSE) obtained in Fig. 10 was 0.315. This result proved that the precision of calculated LAI is as high as that of the measured LAI. However, the error due to shade of mountain should be considered. The open circles in Fig. 10 indicate the relation between calculated LAI and measured LAI in the shade areas of mountain. The error caused by the shade of the mountain mainly occurred in winter. Because of the shade of the mountain, the calculated LAI values from ASTER data in winter were likely lower than the measured LAI.

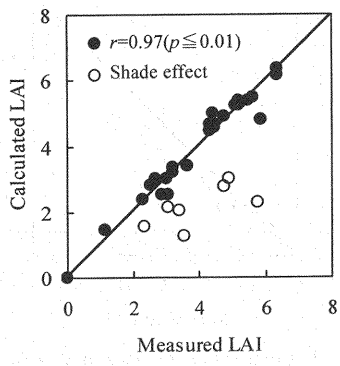

Fig. 10 Comparison of measured LAI and calculated one based on ASTER data at the

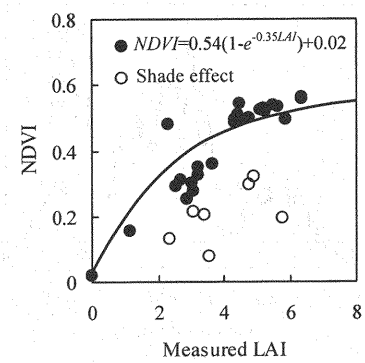

Fig. 11 Relationship between measured LAI and NDVI at observation points

Moreover, we compared the measured LAI and NDVI (NDVI=$(\rho_3-\rho_2)/(\rho_3+\rho_2)$, where, ρ_i=reflectance of i band) which was obtained from ASTER data. As a result, a correlative curve of the exponential function (see Fig. 11) was obtained for the observation area. The RMSE obtained in Fig. 11 was 1.808. The semi-experiential LAI estimation formula using a vegetation index was one of the methods used frequently to estimate LAI using remote sensing technology. However, as illustrated in Fig. 11, the precision of the LAI estimation equation using NDVI is not noticeably high because NDVI increased towards a certain value as LAI increased, and its increase rate is low in the range of high LAI value. On the other hand, the estimation method proposed in this study yielded a good result even at high LAI value. In this study, the atmosphere calibration was carried out by adopting the histogram minimum method (25) which is one of the most simple atmosphere calibration methods.

The LAI distributions in summer and winter on the target region were remarkably different (see Fig. 12). The LAI values in summer and winter ranged 3~7 and 1~4, respectively. The average value of LAI in summer and winter were 4.5 and 2.2, respectively. The LAI distribution maps in summer and winter showed low LAI values from 1 to 2 in many places in spite of timberland. In particular, this result typically appeared more frequently in winter than in summer because of the mountain shade caused by the sun elevation at 11:10 a.m. at the time when the satellite passed. The sun's elevations were 63.9° and 31.6° at the time when the Terra satellite passed on August 18, 2007 and January 9, 2008, respectively.

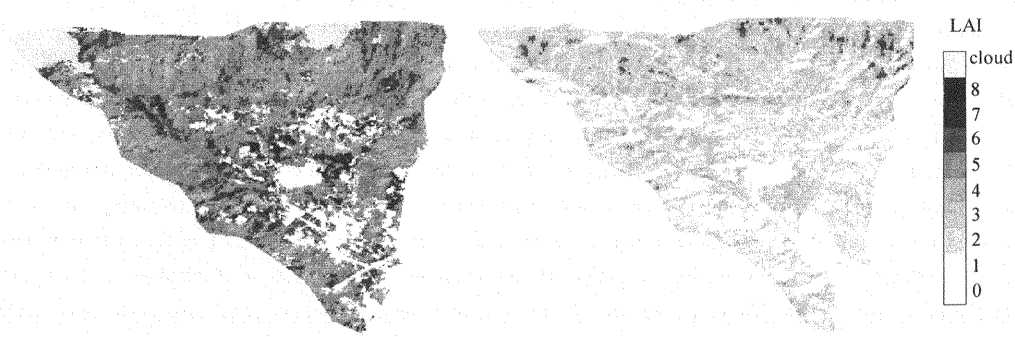

LAI distribution (August 18, 2007)　　LAI distribution (January 9, 2008)

Fig. 12 Distribution of estimated LAI derived from ASTER data in summer and winter

As confirmed by the distribution of mountain shade from the satellite image in the observation area, the satellite images include distributions of the mountain shade of 3.6% and 10.3% in summer and winter, respectively. When we calculated LAI from the satellite image in winter, it was thought that the serious calculation error occurred due to the effect of mountain shade. The difference of LAI distribution in summer and winter is thought to reflect the significant difference in the density of leaves and metabolic activity on the forest in both seasons. Accordingly, this difference of LAI distribution in these two seasons is also considered to be influenced by the transpiration or water circulation process. Furthermore, the distributions of the estimated LAI in summer and winter on the target area are different because of the differences in the density of leaves and metabolic activity during these two seasons.

REFERENCES

1. Chen, J. M., Black, T. A. : Defining leaf area index for non-flat leaves, Plant Cell Environment, Vol.15, No.4, pp.421-429, 1992.
2. Clough, B. F., Ong, J. E., Gong, G. W. : Estimating leaf area index and photosynthetic production in canopies of the mangrove Rhizophora apiculata, Marine Ecology Progress Series, Vol.159, No.1, pp.285-292, 1997.
3. Chason, J. W., Baldocchi, D. D., Huston, M. A. : A comparison of direct and indirect methods for estimating forest canopy leaf area, Agricultural and Forest Meteorology, Vol.57, pp.107-128, 1991.
4. Macfarlane, C., Arndt, S. K., Livesley, S. J., Edgar, A. C., White, D. A., Adams, M. A., Eamus, D. : Estimation of leaf area index in eucalypt forest with vertical foliage, using cover and full frame fisheye photography, Forest Ecology and Management , Vol.242, No.2, pp.756-763, 2007.
5. Barclay, H. J., Trofymow, J. A., Leach, R. I. : Assessing bias from boles in calculating leaf area index in immature Douglas-fir with the LI-COR canopy analyzer, Agricultural and Forest Meteorology, Vol.100, pp.255-260, 2000.
6. Curran, P. J., Steven, M. D. : Multispectral remote sensing for the estimation of green leaf area index, Philosophical Transactions of the Royal Society, Vol.309, No.1508, pp.257-270, 1983.
7. Privette, J. L., Emery, W. J., Schimel, D. S. : Inversion of a vegetation reflectance model with NOAA AVHRR data, Remote Sensing of Environment, Vol.58, No.2, pp.187-200, 1996.
8. Edmund, P. G., Peter, J. M., Alaisdair, J. E., Chris, D. C., Angie, C. E. : Estimating leaf area index of mangroves from satellite data, Aquatic Botany, Vol.58, No.1, pp.11-19, 1997.
9. Price, J. C. : Estimating leaf area index from satellite data, IEEE Transactions on Geoscience and Remote Sensing, Vol.31, No.3, pp.727-734, 1993.
10. Fassnacht, K. S., Gower, S. T., Mackenzie, M. D., Norman, J. M., Lillesand, T. M. : Estimating the leaf area index of north central Wisconsin forest using the landsat thematic mapper, Remote Sensing of Environment, Vol.61, pp.229-245, 1997.
11. Quan, W., Smuel, A., John, T., Andre, G. : On the relationship of NDVI with leaf area index in a deciduous forest site, Remote Sensing of Environment, Vol.94, No.2, pp.244-255, 2004.
12. Duchemin, B., Hadria, R., Erraki, S., Boulet, G., Maisongrande, P., Chehbouni, A., Escadafal, R. : Monitoring wheat phenology and irrigation in Central Morocco, Agricultural Water Management, Vol.79, No.1, pp.1-27, 2006.
13. Seguchi, M. : Estimation of Spatial Distribution of Vegetation Amount in a Watershed Using Landsat-5 TM Image Data, Journal of Hydroscience and Hydraulic Engineering, Vol.38, pp.777-782, 1994 (in Japanese).
14. Yamamoto, H., Suzuki, Y., Hayakawa, M. : A Leaf Area Index Diagnosis by the Transmitted Light, Agricultural Technique System Crops, Rural Culture Association, Vol.16, pp.27-33, 1994 (in Japanese).
15. Abrams, M. : The Advanced Spaceborne Thermal Emission and Reflection radiometer (ASTER): Data products for the high spatial resolution imager on NASA's Terra platform, International Journal of Remote Sensing, Vol.21,

No.5, pp.847-853, 2000.

16. Fujisada, H. : ASTER level 1 data processing algorithm, IEEE Transactions on Geoscience and Remote Sensing, Vol.36, No.4, pp.1101-1112, 1998.
17. Price, J. C. : Estimating vegetation amount from visible and near infrared reflectances, Remote Sensing of Environment, Vol.41, pp29-34, 1992.
18. Sellers, P. J. : Vegetation-canopy spectral reflectance and biophysical processes, In Asrar, G. (Ed.), Theory and applications of optical remote sensing (pp.297-335), John Wiley & Sons, N.Y., 1989.
19. Watanabe, R. : Vegetation and atmosphere, In Kondo, J. (Ed.), Meteorology of the water environment - The earth surface water balance heat balance (pp.208-239), Asakura, Tokyo, 1994 (in Japanese).
20. Huete, A. R. : A soil adjusted vegetation index (SAVI), Remote Sensing of Environment, Vol.25, pp.295-309, 1988.
21. Seguchi, M., Watanabe, K., Hayashi, T. : Basic Studies on the Extraction of Soil and Vegetation Informations of a Basin Using Remote Sensing, Journal of Hydroscience and Hydraulic Engineering, Vol.35, pp.237-242, 1991 (in Japanese).
22. Barent, F., Jacquemond, S., Hanocq, J. F. : The soil line concept in remote sensing, Remote Sensing Reviews, Vol.7, pp.65-82, 1993.
23. Richardson, A. J., Wiegand, C. L. : Distinguishing vegetation from soil background information, Photogrammetric Engineering Remote Sensing, Vol.43, pp.1541-1552, 1977.
24. Buhe, A., Takada, M. : Application to the Field of Environment Using Remote Sensing and GIS Technology, Remote Sensing Seminar in Hokkaido, Satellite Remote Sensing Local Applied Result Report, pp.37-42, 2005 (in Japanese).
25. Campbell, J.B. : Introduction to remote sensing, Guilford press, N.Y., 1987.

APPENDIX – NOTATION

The following symbols are used in this paper:

α = absorption coefficient;

a' = soil line slope;

β = scattering (reflection) coefficient;

b' = soil line intercept;

$BN_{\alpha i}$ = ASTER data of i band correspond to the reflectance above the highest canopy density (R_α);

BN_{si} = ASTER data of i band correspond to the reflectance of the soil surface (R_s);

c = attenuation coefficient;

e_0 = offset coefficient of ASTER sensor;

e_1 = gain coefficient of ASTER sensor;

I = downward radiation in the plant canopy;

J = upward radiation in the plant canopy;

l = thickness of layer from the top of the canopy to the bottom side of the canopy;

L_k = spectral reflection energy;

L'_k = calibration spectral reflection energy;

R = reflectance from the plant canopy;

R_∞ = reflectance from the highest canopy density;

R_s = reflectance from the soil surface;

S = reflectance observed with satellite sensor;

σ = reflectance of atmosphere;

τ = absorption rate of atmosphere;

W = spectral reflection energy of standard reflection plate at the measurement of L_k; and

W_0 = spectral reflection energy of standard reflection plate at culmination.

(Received Aug, 03, 2009 ; revised May, 06, 2010)